This paper has been accepted for publication in IEEE Transactions on Robotics. DOI: 10.1109/TRO.2020.3045644

IEEE Explore: https://ieeexplore.ieee.org/document/9316238

Please cite the paper as:

Joseph Norby, Jun Yang Li, Cameron Selby, Amir Patel, and Aaron M. Johnson, "Enabling Dynamic Behaviors with Aerodynamic Drag in Lightweight Tails," in *IEEE Transactions on Robotics*, 2021.

©2021 IEEE. Personal use of this material is permitted. Permission from IEEE must be obtained for all other uses, in any current or future media, including reprinting/republishing this material for advertising or promotional purposes, creating new collective works, for resale or redistribution to servers or lists, or reuse of any copyrighted component of this work in other works. DOI: 10.1109/TRO.2020.3045644

Enabling Dynamic Behaviors with Aerodynamic Drag in Lightweight Tails

Joseph Norby, Student Member, IEEE, Jun Yang Li, Cameron Selby, Amir Patel, Member, IEEE, and Aaron M. Johnson, Senior Member, IEEE

Abstract—Many agile legged animals employ lightweight, furry tails to regulate orientation during running, leaping, and turning. Most robots attempting the same tasks either lack a tail or employ one with high inertia which can induce impractical payload and energy costs. Inspired by nature's solution to this trade-off, we explore the use of aerodynamic drag tails in reorientation tasks. We present a model of the aerodynamic drag and from this derive a metric that allows for direct comparison between aerodynamic and inertial tails. Motivated by this model, we construct a tail to maximize this effectiveness while minimizing inertia. We demonstrate the utility of this tail for two dynamic behaviors executed on a quadrupedal robot. First, in aerial reorientation the robot achieves a 90 degree rotation within one body length of fall at the same performance as an inertial tail but with just 37% of the normalized inertia. Second, the forward acceleration of the robot is improved by 12% despite increasing the system mass by 10% over a tailless version. These results show that aerodynamic drag can provide significant control authority for a robot while decreasing the payload and energy cost.

Index Terms—Biologically-Inspired Robots, Mechanism Design, Dynamics, Legged Robots.

I. Introduction

TERRESTRIAL animals often use tails to help a wide variety of behaviors that are traditionally challenging for robots. Agama lizards use their long, heavy tails to reorient in mid-air after unexpected foot slip, a failure mode which is often fatal for legged robots [1,2]. Kangaroos use their tails for stability when hopping and even support themselves with their tails while walking [3,4]. Although humans do not have tails, we swing our arms to the same effect while walking and running, increasing both lateral balance and energy efficiency [5].

While these animals exhibit impressive behaviors, none approach cheetahs in terms of speed and agility. A cheetah chasing prey can reach a top speed of 29 m/s and accelerate, decelerate, or turn at rates almost double that of horses [6]. These dynamic maneuvers require very precise regulation of

This work was supported by the National Science Foundation under Grant No. DGE-1745016 and Grant No. IIS-1704256, the Oppenheimer Memorial Trust Fellowship, and the National Research Foundation of South Africa Grant No. 99380. Any opinions, findings, and conclusions or recommendations expressed in this material are those of the author(s) and do not necessarily reflect the views of the National Science Foundation.

J. Norby, J. Y. Li, C. Selby, and A.M. Johnson are with the Department of Mechanical Engineering, Carnegie Mellon University, Pittsburgh, PA, 15213 USA (e-mail: jnorby@andrew.cmu.edu; peter-junyang@hotmail.com; cselby@alumni.cmu.edu; amj1@cmu.edu).

A. Patel is with the Department of Electrical Engineering, University of Cape Town, Private Bag X3, Rondebosch, 7701 South Africa (email: a.patel@uct.ac.za).



Fig. 1. Examples of biological and robotic systems with long aerodynamic tails. The cheetah, the giant Indian squirrel, and the jerboa have tails ranging from 75% to nearly 200% of their body length, motivating the aerodynamic tail presented here. Top left: Cheetah (*Acinonyx jubatus*). Bottom left: Greater Egyptian jerboa (*Jaculus orientalis*), photo credit: Elias Neideck/CC BY-SA 3.0. Middle: Giant Indian squirrel (*Ratufa indica*), photo credit: VinodB-hattu/CC BY-SA 4.0. Right: The Ghost Robotics Minitaur [21], equipped with a 2x body length aerodynamic tail.

angular momentum to maintain balance, avoid foot slip, and accommodate the large reaction forces and moments generated by the legs. Cheetahs have been observed to flick their tails to aid this angular momentum regulation, particularly while decelerating and turning, as shown in Fig. 1 and in [7,8].

Inspired by the ability of these and other tailed animals, researchers have replicated similar tasks on robotic systems. The first known application of a tail in robotics was the Uniroo [9], a running robot that employed a tail to stabilize pitch. This example has since inspired orientation stabilization tails in many legged robots [10–12]. Platforms such as the Berkeley Tailbot, the MSU Tailbot, and Penn RHex have employed tails to successfully perform aerial self-righting maneuvers similar to the Agama lizard [13–15]. Some robots employ tails for aiding more dynamic tasks similar to those perfected by the cheetah, including accelerating and decelerating [8] or turning [7,16,17]. Tails have also been used in other platforms as the primary mechanism for injecting energy into a gait rather than simply augmenting locomotion [18–20].

Despite these achievements, few robots are equipped with tails outside of research focused on the dynamics of tailed locomotion. This is largely due to the added mass and system complexity associated with the tail. Each of the robots highlighted above employ their tails for inertial reorientation [15] – leveraging the high inertia of the tail to allow the motor to do work to reorient the body before the tail exhausts its range of

©2021 IEEE. Personal use of this material is permitted. Permission from IEEE must be obtained for all other uses, in any current or future media, including reprinting/republishing this material for advertising or promotional purposes, creating new collective works, for resale or redistribution to servers or lists, or reuse of any copyrighted component of this work in other works. DOI: 10.1109/TRO.2020.3045644

motion. This means that effective tails must have high inertia, which often does not comply with the tight payload budgets of mobile robots. In contrast, cheetah tails weigh roughly 2% of their body mass, with most of the mass in muscle at the base of the tail resulting in low inertia [22,23].

One hypothesis for the utility of cheetah tails suggests they perform aerodynamic rather than inertial reorientation [22]. Most mammal tails are covered in fur, including those shown in Fig. 1, which increases their aerodynamic drag. When flicked or when moving through a steady airstream, the drag force resists the motion and allows for the application of wrenches to the body. Since this mechanism does not depend on mass, an aerodynamic drag tail can be extremely lightweight compared to an inertial tail. Aerodynamic drag tails have been shown to enable rapid turning on centimeter scale robots [24], although this turning was achieved by fixing the tail at an angle to act as a rudder, or dynamically actuated with all effects attributed to inertial reorientation rather than aerodynamic effects. To the knowledge of the authors, no other studies have investigated actuated aerodynamic effects or offered any comparative analysis for terrestrial tails.

This work investigates the extent to which aerodynamic drag affects the utility of tails in performing dynamic tasks. We present a model (Section II) that captures the dynamics of aerodynamic tails. Then we use that model to show when aerodynamic drag is a significant contribution to control affordance compared to just inertial effects (Section III). Leveraging this model, we constructed a tail (Section IV) to maximize aerodynamic drag while minimizing inertia, shown in Fig. 1 along with several of the animals inspiring its design. Using this tail we demonstrate two biologically motivated behaviors on a robot, aerial self-righting and forward acceleration (Section V) to show applications of this control affordance. Finally, we highlight the practical advantages aerodynamic drag tails exhibit over inertial tails (Section VI).

II. AERODYNAMIC REORIENTATION MODEL

Investigating the utility of aerodynamic drag forces in reorientation tasks requires a model to isolate and compare the aerodynamic and inertial effects. Such a model has been thoroughly researched for inertial reorientation [15] but has not been developed for aerodynamic reorientation. The main result of this work is a model for aerodynamic reorientation and an accompanying metric for effectiveness, from which several insights into the dynamics and utility of aerodynamic drag tails are gleaned.

We model the tail as a non-porous rigid body moving at a relatively high velocity through a fluid, which applies a quadratic drag force [25] according to the relationship

$$F_D = \frac{1}{2}\rho C_D A v^2 \tag{1}$$

where F_D is the aerodynamic drag force acting in the opposite direction of motion, ρ is the density of the fluid, C_D is the drag coefficient that captures the surface interaction between the fluid and the body, A is the surface area of the body, and v is the component of the velocity of the body orthogonal to the surface area.

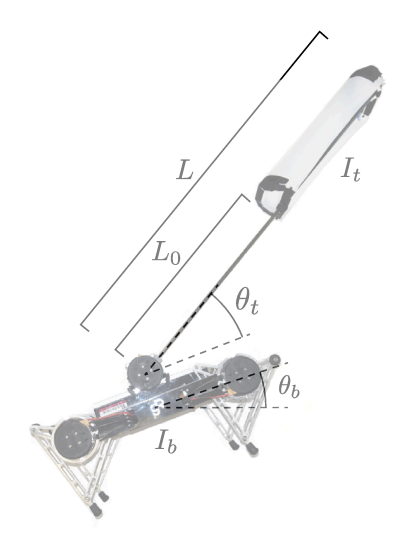


Fig. 2. Schematic of tail system parameters. These parameters describe the tail geometry and model variables used to calculate effectiveness. Not labeled is tail width, w, which is into the page. The geometry of this particular tail is a half cylinder with diameter w, but the model in (2) is not restricted to any one tail shape.

The tail is pinned to a second rigid body (hereafter referred to as "the body") with no other external wrenches, such that the aerodynamic drag force applies a moment to the body. For simplicity we assume the tail velocity is purely determined by its angular velocity and that the aerodynamic drag force F_D is defined in the coordinate frame of the tail such that it is orthogonal to tail motion and therefore independent of the angular position of the tail. These modeling decisions serve to isolate rotation and ignore any translational motion for the sake of clarity, although translational effects would benefit high speed systems as described in [22] and further discussed in Section VI. Integrating this moment along the length of the tail yields a net aerodynamic torque of

$$|\tau_D| = \int_A F_D l \, dA$$

$$= \int_{L_0}^L \frac{1}{2} \rho C_D w ((\dot{\theta}_b + \dot{\theta}_t) l)^2 l \, dl$$

$$= \frac{1}{8} \rho C_D w (\dot{\theta}_b + \dot{\theta}_t)^2 (L^4 - L_0^4)$$
 (2)

where τ_D is the aerodynamic torque applied in the opposite direction of the tail rotation, w is the width of the tail (assumed constant over the length of the tail), L is the length of the tail, L_0 is the distance from the pin joint to the segment of the tail that generates drag, θ_b is the angle of the body with respect to the world frame, and θ_t is the angle of the tail with respect to the body. These parameters are shown in Fig. 2 for an example tail geometry, although this model can apply to other tail geometries so long as the corresponding drag coefficient is known.

This equation highlights the favorable scaling of aerodynamic drag tails, as the drag torque scales with L^4 , or L^5 if tail width is assumed to scale with length. This favorable scaling is reflected in nature through animals like the cheetah, the giant Indian squirrel, or the jerboa, all of which have

furry tails ranging from 75% to nearly twice body length, shown in Fig. 1 [22,26,27]. Quartic length scaling underscores the importance of drag near the tail tip rather than the base, which is particularly notable in the jerboa's tuft of fur at the tip of its relatively thin tail. This equation also highlights favorable quadratic scaling with tail angular velocity, and linear scaling with width and drag coefficient. Mass and inertia are notably absent in this equation, suggesting that effective tails should be long yet lightweight and employed at high speeds. These factors are again consistent with many agile animals, particularly the cheetah [7].

III. COMPARISON OF INERTIAL AND AERODYNAMIC **EFFECTIVENESS**

Equation (2) highlights the important characteristics of aerodynamic drag tails, but does not immediately prescribe the magnitude of the control authority these tails provide. For purely inertial tails, this control authority has been quantified via tail effectiveness ξ , which is defined as the ratio of body rotation to tail rotation under the assumption of constant total angular momentum [15]. For inertial tails, effectiveness is a straightforward function of the tail and body inertias. However, the nonlinearities of the aerodynamics in (2) necessitate numerical methods to quantify effectiveness for an aerodynamic drag tail. We investigate this by constructing the equations of motion of the system in Fig. 2,

$$\begin{bmatrix} I_b + I_t & I_t \\ I_t & I_t \end{bmatrix} \begin{bmatrix} \ddot{\theta}_b \\ \ddot{\theta}_t \end{bmatrix} = \begin{bmatrix} \tau_D \\ G\tau + \tau_D \end{bmatrix}$$
(3)
$$\begin{bmatrix} \ddot{\theta}_b \\ \ddot{\theta}_t \end{bmatrix} = \begin{bmatrix} -\frac{G\tau}{I_b} \\ \frac{I_b + I_t}{I_c I_c} G\tau + \frac{1}{I_c} \tau_D \end{bmatrix}$$
(4)

where I_b and I_t are the body and tail inertias respectively and both defined with respect to the rotational joint, τ is the torque provided by the motor, and G is the gear ratio. We neglect the rotor reflected inertia since optimal gearing for the systems considered here result in reflected inertias much less than that of the tail. Numerically integrating these equations with initial conditions at rest yields the time evolution of the body and tail angles. Together, these quantities define the same tail effectiveness metric as in [15] - the ratio of the body angle achieved to the tail angle swept – but here based on a particular behavior and control input.

We define a baseline task of aerial reorientation similar to that studied in [15] which provides a particular measure of effectiveness. The task is to maximize body rotation in the time it would take for the system to fall one body length, motivated by recovering in mid-air from a fall off a ledge or a leap onto a surface. In addition to the task, aerodynamic tail effectiveness is a function of the gear ratio, actuator, and the tail geometry, as well as the body and tail inertias. To explore these relationships we select a body scale of a common quadrupedal robot, the Ghost Robotics Minitaur [21], and highlight 1x, 1.5x, and 2x body length tails. All tails are modeled as half cylinders with closed ends to maximize the drag coefficient [28], with width w equal to half of the robot body width. The parameters used for this simulation are shown in Table I.

The equations of motion in (4) are integrated from rest with ode45 in MATLAB R2018b to calculate the effectiveness metric. The tail is allowed to rotate freely for the specified duration or until $\theta_t = 180^{\circ}$ at which point the simulation is paused and a plastic impact is applied between the tail and the robot such that the tail is brought to rest and angular momentum is instantaneously conserved. The system is then resumed until the end of the duration.

For each tail length, the optimal gear ratio is found by performing an integer line search, simulating the behavior with each gear ratio from one to 50 then choosing that which produced the highest resulting effectiveness. The torque τ is calculated at each instant with the following motor model:

$$i = \frac{V - k_t G \dot{\theta}_t}{R}$$

$$\tau = f(i)$$

$$f^{-1}(\tau) = 0.539\tau^3 + 8.93\tau$$
(5)
(6)

$$\tau = f(i) \tag{6}$$

$$f^{-1}(\tau) = 0.539\tau^3 + 8.93\tau\tag{7}$$

where i is the current through the motor armature, V is the battery voltage, k_t is the motor torque constant, R is the resistance of the motor, and f(i) is a function that maps current to torque. The values of these parameters are shown in Table I. The inverse of f shown in (7) is obtained by fitting a cubic polynomial to the empirical torque-current relationship given in [19] for the motor (T-motor U8 KV100). This nonlinearity is included to approximate the significant magnetic saturation these motors experience at high currents. This motor model reflects the chosen platform but also captures the general torque-speed relationship of a DC motor.

Specifying the body inertia, tail geometry, and actuation model along with the optimal gear ratio allows for exploration of the relative effect of tail inertia and aerodynamics on effectiveness. We normalize the tail inertia I_t by the total inertia $I_b + I_t$ and sweep across a range of inertias to find the resulting body angle displacements. For each inertia, the effectiveness is calculated both with and without aerodynamic drag to obtain the pure inertial effectiveness and the combined effectiveness, such that the difference between the two defines the aerodynamic contribution. Fig. 3 shows these results.

At low tail inertia, most of the effectiveness of the tail comes from aerodynamic drag. As the inertia increases, the the impact caused by the finite range of motion of the tail increases enough to decrease overall effectiveness – this is quite different from inertial tails that always benefit from increasing inertia. As the inertia increases further, the tail acceleration and velocity decrease which allows for larger torques to be applied for a longer duration. This effect eventually outweighs the reduced aerodynamic component and the induced impact cost, causing the total effectiveness to increase again but only for significantly higher inertias. A purely inertial tail would require almost twice the inertia of the body itself to match the effectiveness of the longest massless aerodynamic drag tail.

The importance of tail length in aerodynamic effectiveness is highlighted in Fig. 3. The short tail maintains a notable improvement in effectiveness for relatively low inertias, but the long tail maintains a significant margin of improvement for a wide range of inertias, yielding a 50% or greater

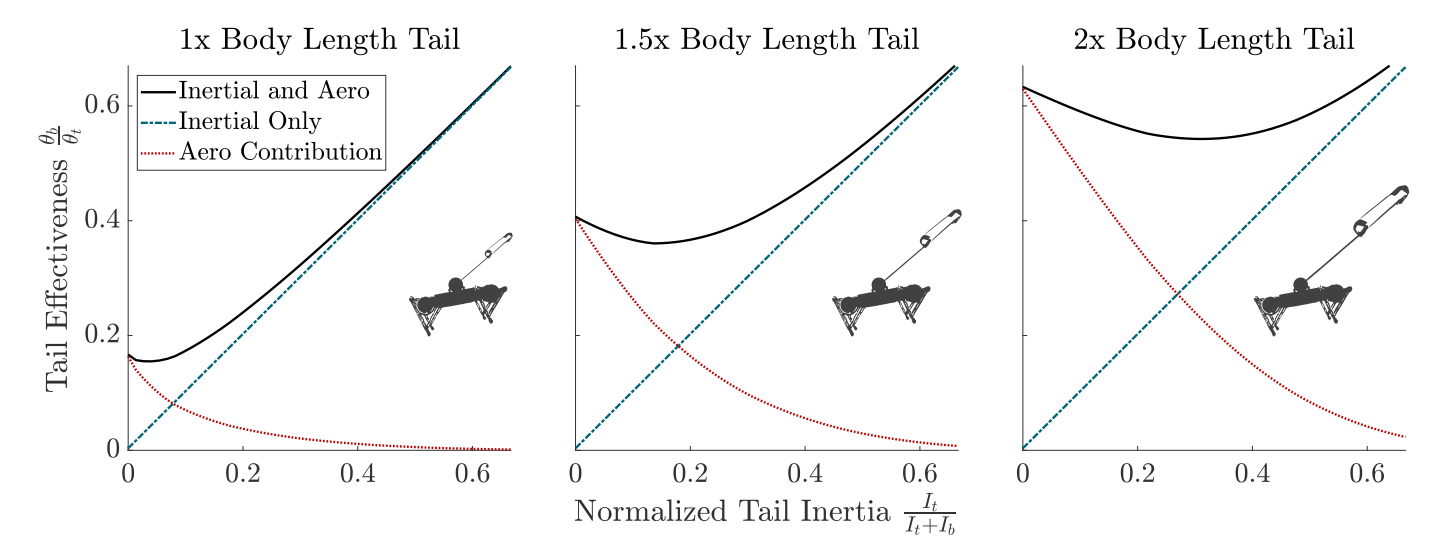


Fig. 3. Aerodynamic effectiveness for various tail lengths and inertias. Aerodynamic drag yields highly effective tails for low inertia. When aerodynamics are not considered, effectiveness (dash-dotted line

) is a function of only normalized tail inertia and independent of tail geometry. When enabled, effectiveness of the tail

increases significantly (colid line). The core dynamic common of the detail line is a constant.

increases significantly (solid line). The aerodynamic component (dotted line) is equal to the total effectiveness minus the inertial effectiveness. Each plot indicates the tail length used to calculate effectiveness.

improvement in effectiveness up to a tail normalized inertia of 0.37, or roughly half the body inertia. The long tail is almost four times as effective as the short tail in the massless case. This underscores the importance of length over mass in aerodynamic tail design. Both lighter and longer tails allow for increased tail tip velocities and improved effectiveness. This is a favorable trend for both biology and robotics, as lighter appendages allow for more agile behaviors and increase the allowable payload of the system.

Other properties of the tail such as width w, tail shaft length L_0 , and the tail geometry (i.e. the corresponding drag coefficient) all affect aerodynamic effectiveness in addition to tail length. Equation (2) also exposes the effects of these additional properties. Aerodynamic torque scales linearly with width and drag coefficient, so these quantities should be maximized subject to relevant design constraints. Tail shaft length is optimal at $L_0=0$ m, but due to its quartic scaling the aerodynamic torque is only significantly reduced for values of L_0 close to L, as shown in Fig. 4. Other design factors such as the weight of the tail material or the tail rigidity may encourage larger values of L_0 , so a designer must strike a balance between these design choices and optimality.

IV. HARDWARE IMPLEMENTATION

Verifying the model results above in hardware requires a highly effective tail to maximize drag. As previously discussed, aerodynamic effectiveness is dependent on tail geometry and in particular the drag coefficient, C_d . The drag coefficient is a dimensionless measure of resistance of a body to transverse fluid flow. In biological tails, fur increases this resistance substantially without adding significant mass to the tail [22]. Engineered tails have more flexibility in their design, and can employ other geometries and materials to maximize drag and minimize mass.

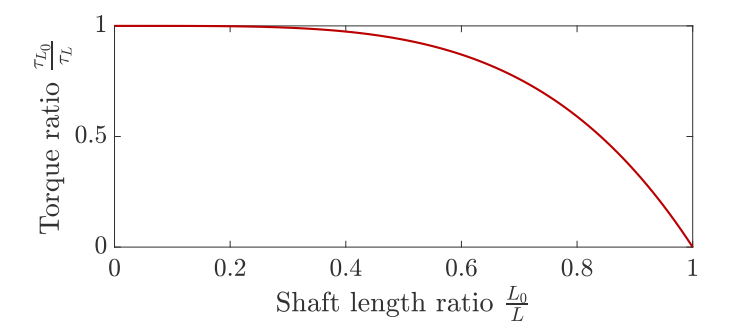


Fig. 4. The effect of tail shaft length on the aerodynamic drag torque for a constant overall tail length L. The applied torque decreases with increasing tail shaft length L_0 , but the quartic scaling results in a significant reduction only for values of L_0 close to L. The x-axis here shows the ratio of the tail shaft L_0 to the total length L, and is equivalent to the fraction of the tail that produces no aerodynamic drag. The y-axis describes the ratio of the torque τ_{L_0} produced by a tail of length L with shaft length L_0 to the torque τ_L produced by a tail of length L with $L_0=0$.

The tail constructed for the aerial self-righting and forward acceleration tasks presented here features a 1 m long (2x body length), 1 cm diameter carbon fiber shaft (2159T85 McMaster-Carr) fitted with a 18 cm wide UHMW polyethylene film (85655K13 McMaster-Carr) half cylinder scoop at the end. These materials were selected for their high strength-to-weight ratios. The ends of the scoop were sealed to prevent air from escaping radially. The whole tail weighs 110 g with an inertia of 0.058 kg·m2, which when normalized for the tested hardware platform yields a normalized tail inertia of 0.204. The tail is rigidly mounted to the output of a planetary geartrain driven by a U8 motor, which in turn is fixed to the robot chassis. The optimality of the gear ratio was determined by the process outlined in Section III. These and other hardware parameters are listed in Table I, and the tail can be seen in Figs. 1 and 2.

TABLE I ROBOT, TAIL, AND ACTUATOR PARAMETERS

Parameter	Symbol	Value	Units
Body mass	_	7.3	kg
Body length	_	0.50	m
Body inertia	I_b	0.23	$kg \cdot m^2$
Tail framing mass	-	0.706	kg
Tail mass	_	0.110	kg
Tail length	L	1.0	m
Tail shaft length	L_0	0.60	m
Tail width	w	0.18	m
Tail inertia	I_t	0.058	$kg \cdot m^2$
Tail normalized inertia	$\frac{I_t}{I_t + I_b}$	0.204	-
Tail gear ratio	G	4:1	-
Tail drag coefficient	C_D	2.0	-
Motor torque constant	k_t	0.0954	$\frac{\mathbf{N} \cdot \mathbf{m}}{\mathbf{A}}$
Motor winding resistance	R	0.186	Ω
Motor voltage	V	16	V

It should be reiterated that these values for L, L_0 , and w are not optimal for aerodynamic effectiveness, as optimality would be achieved with $L=\infty$, $L_0=0$, and $w=\infty$. These parameters are bounded by other design constraints which a roboticist may select for a particular application. In this case we prioritize a reasonable motion envelope and tail rigidity, and therefore restrict the tail length as inspired by the animals in Fig. 1, and the tail width and shaft length to maintain rigidity in the UHMW film.

To calculate the drag coefficient of this tail, a smaller tail with the same shape was fixed to the motor used in the above experiments, and spun freely with different voltages to produce steady state angular velocities. The resulting aerodynamic torque was then calculated by measuring the current and voltage supplied to the motor and equating the electrical power input to the sum of the resistive losses in the motor and the mechanical power output to yield the aerodynamic torque. This resulted in a torque-angular velocity curve which was fit to a quadratic as shown in Fig. 5, with $R^2 = 0.977$ indicating good quadratic fit. Matching this curve to that in (2) and accounting for the tail dimensions yields a drag coefficient of 2.0, slightly less than the theoretical value of 2.3 [28].

V. EXPERIMENTAL RESULTS

To verify these model results and highlight practical applications for aerodynamic reorientation, we demonstrate two tailassisted tasks: aerial self-righting and forward acceleration. The aerial self-righting task corresponds to the model analysis and shows the utility of expanded control authority, whereas the forward acceleration task tests the ability of the tail to apply this control authority to a dynamic task that requires both linear and rotational motion.

A. Aerial Self-Righting

To verify these model results and highlight practical applications for aerodynamic reorientation, we first demonstrate the use of an aerodynamic drag tail in an aerial self-righting task. This task corresponds directly to the model analysis and

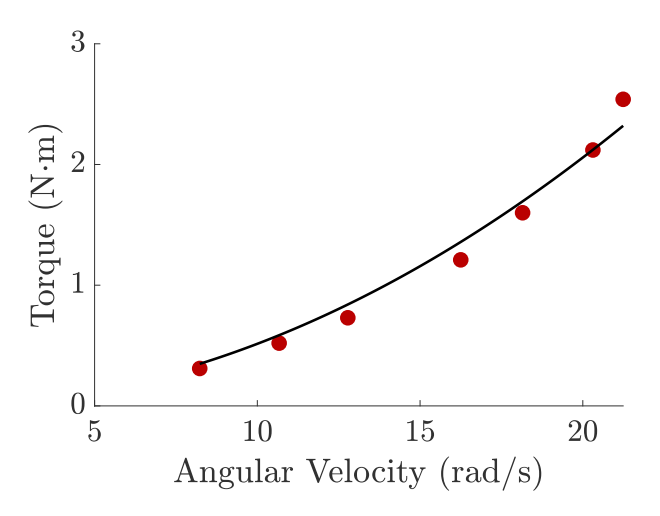


Fig. 5. Experimental validation of drag coefficient and quadratic torque to velocity relationship. Aerodynamic torque produced by a half cylinder aerodynamic drag tail was measured while rotating the tail at various angular velocities. The red dots represent experimental data, and the black line is a quadratic fit given by $\tau_D=0.00514\,\dot{\theta}_t^2,$ with an $R^2=0.977$ indicating good fit.

shows both the utility and the magnitude of expanded control authority such a tail offers.

The aerial self-righting task was executed by dropping the system from a height and providing a step input to the actuator of a 2x body length tail so that the system rotates 90 degrees and lands on its feet. This task was previously tested for robots with inertial tails in [1,15], which were able to successfully land on their feet but required a tail with more inertia than the body to do so. This experiment directly tests the ability of a system to aggressively reorient, as failure to reorient quickly can result in severe damage to the system if it cannot land on its feet.

To perform this experiment, a Ghost Robotics Minitaur was equipped with the previously described aerodynamic drag tail, oriented vertically and dropped from a height of one body length (0.5 m). The drop height was defined as the vertical displacement of the center of mass from the beginning of the drop to the final resting position. The robot was held aloft by a quick release clip activated by pulling a pin that holds the clip in place. This pin was pulled at the same time that the robot was commanded to begin the reorientation behavior. High speed camera footage confirmed that the robot consistently began the reorientation a few milliseconds after the clip was released. Body pitch data was recorded with an Optitrack motion capture system. The resulting pitch trajectory is shown in Fig. 6, and a time sequence of the behavior is shown in Fig. 7. The simulation data in Fig. 6 was synchronized with the experimental data at the last instant before the motion capture data showed a body pitch displacement. This instant occurs a few milliseconds after the step input is provided at t=0 due to backlash in the geartrain and tail deflection. This experiment consisted of four trials to reduce any noise in the data, although Fig. 6 shows that the standard deviation between these trials was very small ($\sigma = 1.5^{\circ}$ on average over the course of the fall).

The robot tracks the model-predicted trajectory well, ro-

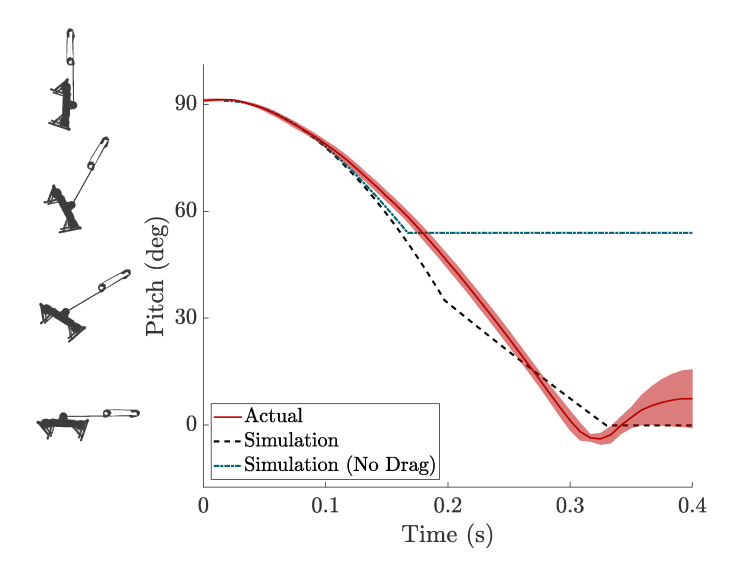


Fig. 6. Aerial self-righting pitch trajectory. Motion capture orientation data during the aerial-self righting task (solid line) show the robot tracking the model predicted trajectory (dashed line) until ground impact, with a slight delay due to unmodeled tail shaft deflection. A simulation of the tail with no aerodynamic drag is included for comparison (dash-dotted line). The discontinuity in the velocity of each tail simulation is caused by the modeled plastic impact between the tail and the robot body, which is significantly more problematic without aerodynamic effects. This discontinuity is not observed in the experimental data as the shaft deflection delayed this impact until just before touchdown and reduced its plasticity. The shaded region represents 1σ variance (N=4).

tating 90 degrees in 302 ms on average (standard deviation of 4 ms). The slight delay in body pitch tracking is likely due to the deflection in the carbon fiber tail shaft, which slows the acceleration of the tail. This rapid reorientation allows the robot to land safely and absorb the impact with its legs rather than its chassis. Without the tail, the robot simply falls straight to the ground, which for falls exceeding a body length can easily damage the robot. Notably, this resulting effectiveness matches that of the inertial tail tested in [15], but with a normalized tail inertia of 0.204 rather than 0.558, a reduction of 63%. A tail of the same inertia as tested but with no drag was simulated, with the resulting trajectory in Fig. 6 indicating only 37 degrees of rotation. Note that in the purely inertial case this effectiveness can be calculated directly from the normalized inertia using the relationship derived in [15] without integration.

B. Forward Acceleration

Lightweight aerodynamic tails are effective at reorientation tasks, but successful biological or robotic locomotion involves a broad range of agile behaviors, such as running, jumping, or turning. Often these behaviors require precise application of large forces into the ground in order to accelerate the body in a desired direction. Equipping a robot with a tail adds mass to the system, which reduces the acceleration a given force produces. However, aerodynamic drag tails provide additional control authority which could be employed to increase the agility of the system.

We leverage trajectory optimization to investigate the effect of aerodynamic drag tails on the forward acceleration of a legged robot. This method represents the motion of the robot with a parameterized trajectory, defines the desired task through constraint functions evaluated on that trajectory, and determines optimality with respect to a cost function. This is a well-studied method in optimal control so we refer to prior literature for details [29–31].

The task encoded here is very similar to the quadruped leaping behavior described in [31], and shares the same constraints on dynamic feasibility, contact schedule, joint and torque limits, friction cones, and initial resting configuration. Unlike [31], we optimize for the forward velocity of the system at liftoff divided by the behavior duration to maximize acceleration. We do not constrain the duration of each contact phase as in [31], although we do apply a lower bound of 1.3 m/s – the average running speed of the robot – to the final forward velocity to replicate a stand-to-run gait transition. Dynamic and kinematic constraint bounds are derived from the Minitaur robot parameters in Table I, the motor model in (5)–(7), and [21]. Separate trajectories are optimized both with and without a tail, which starts at rest. The trajectories are transcribed into a direct collocation hybrid trajectory optimization framework in FROST [32] and solved with IPOPT [33]. Each optimization is seeded with an initial trajectory of the average of the upper and lower bounds on each variable.

The outputs of this process are time-parameterized trajectories of the robot state, joint trajectories and torques (for both the leg and tail motors), and contact forces. These trajectories were tracked on the hardware by replaying the open loop joint torques and applying joint level PD feedback to track the trajectory of each individual joint. Each trajectory was executed six times, and the resulting velocity of each trajectory was measured by recording position with an OptiTrack motion capture system and differentiating the signal with respect to time. The final velocity was defined as the forward velocity of the system after the feet left the ground, and the duration of the behavior was given by the trajectory. Prior to each round of testing, the battery was charged to full voltage and the motors were allowed to cool to ensure external conditions remained consistent. The time sequence of the behavior is shown in Fig. 8, and the resulting velocity trajectories and average accelerations are shown in Fig. 9.

With the long aerodynamic tail, the robot accelerates at 6.3 m/s², 12% faster than the 5.6 m/s² without a tail despite a 10% increase in robot mass. The robot accelerates 18% faster than the 5.3 m/s² if the tail were installed but inactive. This increase is achieved by swinging the tail backwards as the legs prepare for and then execute the forward leap, aided in part by a small amount of forward impulse exerted on the tail (5%) of the total change in momentum of the system). Swinging the tail backwards provides forward thrust on the robot, which allows the legs to extend earlier than without the tail, reducing the time required to reach top speed by 11%. Similarly to the aerial self-righting experiment, a tail of the same inertia as tested but with no drag was simulated. The increase to acceleration from aerodynamic and inertial effects was 23% higher than the increase from purely inertial effects. While this improvement is not of the same magnitude observed in aerial self-righting since the task specified linear motion rather than

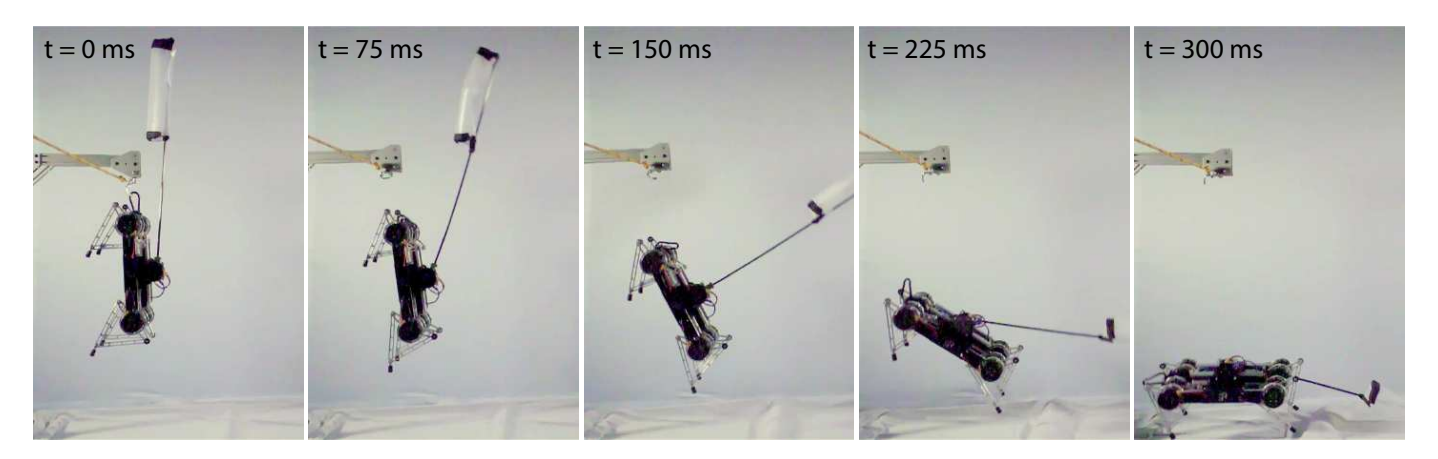


Fig. 7. Aerial self-righting time sequence. The robot rotates from vertical to horizontal in one body length of travel. The first frame shows the moment the robot was released, and the last frame shows the feet of the robot just above the ground. The second frame shows the deflection visible in the tail shaft – despite the deviations from the model induced by this deflection, the robot is still able to rotate a full 90 degrees in one body length of free fall.

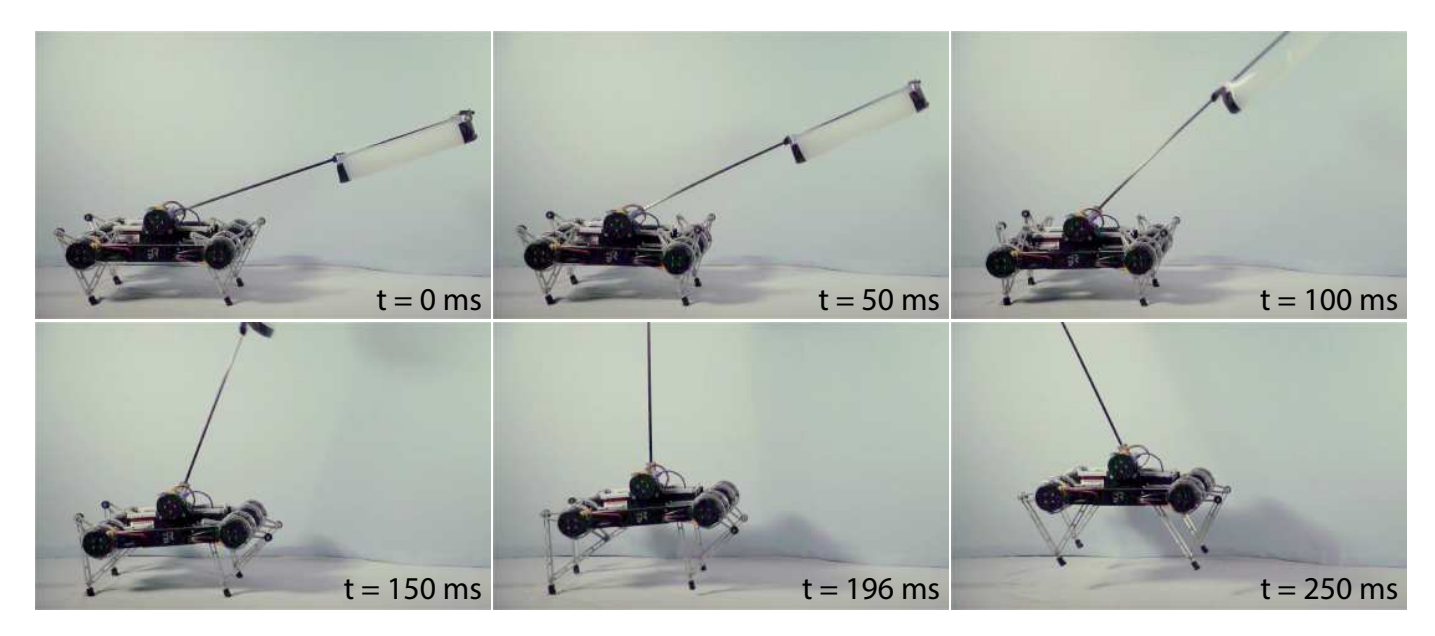


Fig. 8. Forward acceleration behavior time sequence. The time sequence of the acceleration behavior shows the tail swinging backwards, shifting the robot forwards into a position to extend its legs. The behavior ends as the robot's feet lift of the ground at 196 ms. The final frame shows the forward motion after liftoff, although this is not considered in calculating average acceleration.

rotational, it still indicates that aerodynamic effects can bolster the effectiveness of tails in locomotion.

VI. DISCUSSION

The results presented above show that the utility of aerodynamic tails matches and in some cases exceeds that of inertial tails, and in doing so can provide a meaningful contribution to overall system agility. Aerodynamic tails also overcome several shortcomings that often plague inertial tails. Based on the quantitative results shown above and from our experience working with aerodynamic tails, we highlight a few of these key properties.

A. Mass and Inertia

The most evident advantage of aerodynamic tails is their low mass. Since producing aerodynamic drag is independent of mass (unlike inertial reorientation), aerodynamic tails can be extremely lightweight. This increases the available payload of a system, and enables leg forces to produce higher accelerations. Lower tail inertia also reduces the impulse required to arrest tail motion. Inertial tails are capable of rejecting disturbances rapidly by transmitting energy into the tail, but shortly thereafter this energy must be removed, either by applying a counter-torque to slow the tail or from an impact between the tail and the body. This presents a challenging planning problem to precisely regulate the flow of energy from the tail to the body over time. Aerodynamic tails mitigate this issue by providing large amounts of control authority for significantly less tail momentum. Lower mass also reduces the gravitational moment on the tail, requiring less torque to hold the tail in a static position when active control is not required.

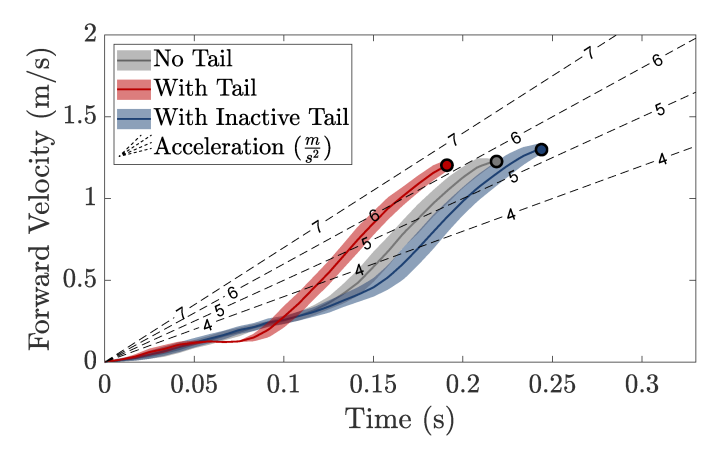


Fig. 9. Forward acceleration behavior trajectories. Experimentally measured robot velocities over time show the robot reaching the same velocity faster with the tail. The shaded region represents 1σ variance (N=6). The dashed lines show the average acceleration to achieve a final velocity over a given duration.

B. External Work

Aerodynamic tails also have a distinct advantage over inertial tails in that they can do work on the environment. This ability allows them to apply continuous torque even at zero acceleration, unlike inertial tails which produce no torque at zero acceleration. This ability also enables non-zero net impulses. Since inertial tails transfer momentum internally between the tail and the body, once the tail sweeps its full range of motion both tail and body return to their initial angular velocity. Lightweight aerodynamic tails can come to rest given a small internal impulse, but due to the net impulse from the environment the body can continue to rotate. This is apparent in the simulation data in Fig. 6. When the purely inertial tail collides with the body all rotation ceases, whereas the impact between the body and the aerodynamic tail (which occurs roughly 180 ms into the simulated self-righting behavior) is much smaller in magnitude, allowing further body rotation.

C. Effectiveness at High Speeds

Aerodynamic tails also benefit from favorable scaling at high speeds. Since both the aerodynamic force and generated moment scale with velocity squared, any tail motions executed while the robot is moving rapidly are amplified. The model derived in (2) can be adjusted to account for these translational effects, producing

$$|\tau_D| = \int_A F_D l \, dA$$

$$= \int_{L_0}^L \frac{1}{2} \rho C_D w((\dot{\theta}_b + \dot{\theta}_t)l + \dots$$

$$\dots - v_x \sin(\theta_b + \theta_t) + v_y \cos(\theta_b + \theta_t))^2 l \, dl, \quad (8)$$

where v_x and v_y are the components of the body velocity expressed in the same spatial coordinate frame that defines body rotation. We omit the closed-form solution of (8) due to its length, but the integrand still highlights how the applied torque scales quadratically with the linear velocity of the body.

This phenomenon has been explored for cheetahs in [22], which showed a 28% improvement to angular impulse while turning at 30 m/s compared to a static airstream. This is useful for legged systems as the high speeds that enable this expanded control authority often require larger magnitudes of actuation for stability.

D. Scaling with Body Length

The scaling analysis offered here has largely been focused on the scaling of the tail length for a fixed body length to highlight the importance of a long and lightweight tail. Isometrically scaling the tail with the body length would also change the tail width, resulting in an aerodynamic torque that scales with L^5 . Interestingly, this matches the scaling of inertia with body length, as inertia scales with mL^2 , where m is the mass of the system and scales with L^3 . This differs from the conclusion in [24] that aerodynamic drag scales with L^3 here we assume that the tail velocity is determined by angular rotation rather than simply forward velocity. This suggests that aerodynamic drag tails can be effective at any scale, although the additional translational effects may be primarily useful at smaller scales, provided that the Reynolds number remains high enough to induce turbulent flow.

E. Limitations

The favorable scaling of aerodynamic drag tails does not come without limitation. Often robots that operate in close quarters have tight restrictions on their workspace, and for such systems a body length or longer tail may be infeasible. Aerodynamic tails also benefit from length and low mass, which induces a design tradeoff between effectiveness and durability – a highly effective tail may not be able to withstand large interaction forces with the environment. These remain open design challenges, although many biological systems employ lightweight, flexible structures to reduce impacts, modify the tail workspace, and increase durability.

Regardless of the inertial or aerodynamic properties of the tail, introducing compliance induces a delay in reorientation as discussed in Section V-A, which is not modeled here due to the rigid body assumption. Applications where knowledge of this delay is critical may necessitate more detailed equations of motion to capture this behavior. This could be achieved with the addition of a passive torsion spring between the motor output and the tail or by directly modeling the tail as a flexible beam rather than a rigid body. This spring should have sufficient stiffness to manage this delay and any associated stability issues.

It should also be emphasized that studying the nonlinear nature of aerodynamic drag requires a prespecified task, actuation model, geometry, and scale, all of which affect the utility of the tail. Despite an effort to isolate each of these components and offer insight into each in turn, the synthesis of these components remains a behavior-specific challenge.

VII. CONCLUSIONS

The favorable scaling of aerodynamic tails make them lightweight yet effective tools to increase the control affor-

dance of a system. This paper presents a model and a corresponding metric to analyze these aerodynamic effects, shows that the magnitude of control affordance can be substantial for long and lightweight tails, and demonstrates this utility in two dynamic behaviors on relevant hardware. A roboticist seeking to overcome underactuation of a system without adding large amounts of mass can thus employ an aerodynamic drag tail by maximizing the components of (2) subject to applicable design constraints. The ability of the aerodynamic drag tail to exert forces directly on the environment coupled with its low momentum compared to the body also makes planning stable motions much simpler. Together, these factors improve the practical implementation of the tail, enabling its application to a wide variety of systems where control authority is critical.

ACKNOWLEDGMENT

The authors would like to acknowledge Ayonga Hereid for his help implementing the FROST framework, Vinay Mitta for his aid in collecting motion capture data, and Adam Zeloof for his aid in modeling tail fur.

REFERENCES

- T. Libby, T. Y. Moore, E. Chang-Siu, D. Li, D. J. Cohen, A. Jusufi, and R. J. Full, "Tail-assisted pitch control in lizards, robots and dinosaurs," *Nature*, vol. 481, no. 7380, pp. 181–184, 2012.
- [2] C. G. Atkeson, P. W. Benzun, N. Banerjee, D. Berenson, C. P. Bove, X. Cui, M. DeDonato, R. Du, S. Feng, P. Franklin, M. Gennert, J. P. Graff, P. He, A. Jaeger, J. Kim, K. Knoedler, L. Li, C. Liu, X. Long, T. Padir, F. Polido, G. G. Tighe, and X. Xinjilefu, "What happened at the DARPA robotics challenge finals," *Springer Tracts Adv. Robot.*, vol. 121, pp. 667–684, 2018.
- [3] R. M. N. Alexander, "The mechanics and energetics of hopping by kangaroos (Macropodidae)," J. Zool., vol. 177, pp. 265–303, 1975.
- [4] J. M. Donelan, S. M. O 'connor, T. J. Dawson, and R. Kram, "The kangaroo's tail propels and powers pentapedal locomotion," *Biol. Lett.*, vol. 10, no. figure 1, pp. 1–4, 2014.
- [5] C. J. Arellano and R. Kram, "The effects of step width and arm swing on energetic cost and lateral balance during running," *J. Biomech.*, vol. 44, no. 7, pp. 1291–1295, 2011.
- [6] A. M. Wilson, J. C. Lowe, K. Roskilly, P. E. Hudson, K. A. Golabek, and J. W. McNutt, "Locomotion dynamics of hunting in wild cheetahs," *Nature*, vol. 498, no. 7453, pp. 185–189, 2013.
- [7] A. Patel and M. Braae, "Rapid turning at high-speed: Inspirations from the cheetah's tail," *IEEE/RSJ Int. Conf. Intell. Robot. Syst.*, pp. 5506– 5511, 2013.
- [8] —, "Rapid acceleration and braking: Inspirations from the cheetah's tail," *IEEE Int. Conf. Robot. Autom.*, pp. 793–799, 2014.
- [9] G. J. Zeglin, "Uniroo-a one legged dynamic hopping robot," Ph.D. dissertation, Massachusetts Institute of Technology, 1991.
- [10] G. H. Liu, H. Y. Lin, H. Y. Lin, S. T. Chen, and P. C. Lin, "A bioinspired hopping kangaroo robot with an active tail," *J. Bionic Eng.*, vol. 11, no. 4, pp. 541–555, 2014.
- [11] R. Briggs, J. Lee, M. Haberland, and S. Kim, "Tails in biomimetic design: Analysis, simulation, and experiment," *IEEE/RSJ Int. Conf. Intell. Robot. Syst.*, pp. 1473–1480, 2012.
- [12] D. W. Haldane, J. K. Yim, and R. S. Fearing, "Repetitive extreme-acceleration (14-g) spatial jumping with Salto-1P," *IEEE/RSJ Int. Conf. Intell. Robot. Syst.*, pp. 3345–3351, 2017.
- [13] E. Chang-Siu, T. Libby, M. Tomizuka, and R. J. Full, "A lizard-inspired active tail enables rapid maneuvers and dynamic stabilization in a terrestrial robot," *IEEE/RSJ Int. Conf. Intell. Robot. Syst.*, pp. 1887– 1894, 2011.
- [14] J. Zhao, T. Zhao, N. Xi, M. W. Mutka, and L. Xiao, "MSU Tailbot: Controlling Aerial Maneuver of a Miniature-Tailed Jumping Robot," *IEEE/ASME Trans. Mechatronics*, vol. 20, no. 6, pp. 2903–2914, 2015.
- [15] T. Libby, A. M. Johnson, E. Chang-Siu, R. J. Full, and D. E. Koditschek, "Comparative Design, Scaling, and Control of Appendages for Inertial Reorientation," *IEEE Trans. Robot.*, vol. 32, no. 6, pp. 1380–1398, 2016.

- [16] N. J. Kohut, A. O. Pullin, D. W. Haldane, D. Zarrouk, and R. S. Fearing, "Precise dynamic turning of a 10 cm legged robot on a low friction surface using a tail," *IEEE Int. Conf. Robot. Autom.*, pp. 3299–3306, 2013.
- [17] C. Casarez, I. Penskiy, and S. Bergbreiter, "Using an inertial tail for rapid turns on a miniature legged robot," *IEEE Int. Conf. Robot. Autom.*, pp. 5469–5474, 2013.
- [18] F. J. Berenguer and F. M. Monasterio-Huelin, "Zappa, a quassi-passive biped walking robot with a tail: Modeling, behavior, and kinematic estimation using accelerometers," *IEEE Trans. Ind. Electron.*, vol. 55, no. 9, pp. 3281–3289, 2008.
- [19] A. De and D. E. Koditschek, "The Penn Jerboa: A platform for exploring parallel composition of templates," arXiv Prepr. arXiv1502.05347, 2015.
- [20] R. Balasubramanian, A. A. Rizzi, and M. T. Mason, "Legless locomotion: A novel locomotion technique for legged robots," *Int. J. Rob. Res.*, vol. 27, no. 5, pp. 575–594, 2008.
- [21] G. Kenneally, A. De, and D. Koditschek, "Design Principles for a Family of Direct-Drive Legged Robots," *IEEE Robot. Autom. Lett.*, vol. 1, no. 2, pp. 900–907, 2016.
- [22] A. Patel, E. Boje, C. Fisher, L. Louis, and E. Lane, "Quasi-steady state aerodynamics of the cheetah tail," *Biol. Open*, vol. 5, no. 8, pp. 1072– 1076, 2016.
- [23] P. E. Hudson, "The structural and functional specialisation of locomotion in the cheetah (Acinonyx jubatus)," Ph.D. dissertation, Royal Veterinary College (University of London), 2011.
- [24] N. J. Kohut, D. Zarrouk, K. C. Peterson, and R. S. Fearing, "Aerodynamic steering of a 10 cm high-speed running robot," *IEEE/RSJ Int. Conf. Intell. Robot. Syst.*, pp. 5593–5599, 2013.
- [25] L. Landau and E. Lifschitz, Fluid mechanics, Series in advanced physics, vol. 6. Addison-Wesley, Reading, MA, 1959.
- [26] H. S. Sushma and M. Singh, "Hunting of Indian giant squirrel (Ratufa indica) by the lion-tailed macaque (Macaca silenus) in the Western Ghats, India," Curr. Sci., vol. 95, no. 11, pp. 1535–1536, 2008.
- [27] D. Happold, "Biology of the jerboa, Jaculus jaculus butleri (Rodentia, Dipodidae), in the Sudan," *Journal of Zoology*, vol. 151, no. 2, pp. 257–275, 1967.
- [28] S. F. Hoerner, "Fluid-dynamic drag," Hoerner Fluid Dynamics, 1965.
- [29] A. Witkin and M. Kass, "Spacetime constraints," ACM Siggraph Computer Graphics, vol. 22, no. 4, pp. 159–168, 1988.
- [30] G. Schultz and K. Mombaur, "Modeling and optimal control of humanlike running," *IEEE/ASME Transactions on mechatronics*, vol. 15, no. 5, pp. 783–792, 2009.
- [31] Q. Nguyen, M. J. Powell, B. Katz, J. Di Carlo, and S. Kim, "Optimized jumping on the mit cheetah 3 robot," in 2019 International Conference on Robotics and Automation (ICRA). IEEE, 2019, pp. 7448–7454.
- [32] A. Hereid and A. D. Ames, "FROST: Fast robot optimization and simulation toolkit," *IEEE/RSJ Int. Conf. Intell. Robot. Syst.*, pp. 719– 726, 2017.
- [33] L. T. Biegler and V. M. Zavala, "Large-scale nonlinear programming using IPOPT: An integrating framework for enterprise-wide dynamic optimization," *Computers & Chemical Engineering*, vol. 33, no. 3, pp. 575–582, 2009.



Joseph Norby (S'19) was born in Minneapolis, MN, USA in 1994. He received the B.S. degree in mechanical engineering from the University of Notre Dame, Notre Dame, IN, USA in 2016. He is currently pursuing the Ph.D. degree in mechanical engineering at Carnegie Mellon University, Pittsburgh, PA, USA.

He was previously a Research Assistant at the Locomotion and Biomechanics Laboratory at the University of Notre Dame, and a Mechanical Engineering Intern with Ziegler CAT. His research

interests include legged locomotion, motion planning, nonlinear controls, and hyrbid dynamical systems.

Mr. Norby is a National Science Foundation Graduate Research Fellow. He is a member of the American Physical Society.



Jun Yang Li received the B.S. degree in mechanical engineering in 2018 and the M.S. degree in mechanical engineering in 2019 from Carnegie Mellon University, Pittsburgh, PA, USA.

From September 2018 to May 2019, he was a Research Assistant at the Robomechanics Lab at Carnegie Mellon University. From 2019 to 2020 he was a Mechanical Designer Intern at HG Tech, Wuhan, China.



Amir Patel (M'13) received the B.S. degree in mechatronics in 2009, the M.S. degree in control engineering in 2011, and the Ph.D. degree in mechatronics in 2014 from the University of Cape Town, Cape Town, South Africa.

He is currently an Associate Professor in the Department of Electrical Engineering at the University of Cape Town, and the director of the African Robotics Unit. He was previously a Visiting Research Scholar at Carnegie Mellon University and Johns Hopkins University, and a Senior Software

Developer with Tellumat. His research interests include maneuverability in legged animals, bioinspired robotics, optimal control, and novel sensing systems.

Dr. Patel was awarded the Claude Leon Merit Award in 2016 and then the Oppenheimer Memorial Trust Fellowship in 2018. He was a runner-up for the IEEE-RAS Technical Committee on Model-Based Optimization for Robotics Best Paper Award in 2019.



Cameron Selby was born in Pittsburgh, PA in 1996. He received the B.S. degree and the M.S. degree in mechanical engineering in 2019 from Carnegie Mellon University, Pittsburgh, PA, USA.

He currently works in the robotics and silicon industries as a Mechanical Engineer at BriteLab Inc. in San Jose, CA. He was previously an Automation Solutions Engineer at Rollon Corporation, and a Mechanical Engineering Intern at Lutron Electronics Co.



Aaron M. Johnson (S'06–M'14-SM'19) was born in Washington, DC, USA. He received the B.S. degree in electrical and computer engineering from Carnegie Mellon University, Pittsburgh, PA, USA, in 2008 and the Ph.D. degree in electrical and systems engineering from University of Pennsylvania, Philadelphia, PA, in 2014.

He is currently an Assistant Professor of Mechanical Engineering at Carnegie Mellon University, with appointments in the Robotics Institute and Electrical and Computer Engineering Department.

He was previously a Postdoctoral Fellow at Carnegie Mellon University and the University of Pennsylvania. His research interests include legged robots, contact-rich manipulation, hybrid dynamical systems, robust control, physics based planning & learning, and bioinspired robotics.

Dr. Johnson is a member of the American Society of Mechanical Engineers and the American Society for Engineering Education. He is an Associate Editor for the IEEE International Conference on Robotics and Automation. He was a runner-up for the IEEE-RAS Technical Committee on Model-Based Optimization for Robotics Best Paper Award in 2019. He received the NSF CAREER award in 2020 and the ARO Young Investigator Award in 2018.